BBA - Biomembranes 1867 (2025) 184424

Contents lists available at ScienceDirect

BBA - Biomembranes

journal homepage: www.elsevier.com/locate/bbamem

Influence of lipid saturation on the structural properties of styrene maleic acid lipid nanoparticles (SMALPs)

Evelyn A. Okorafor [a], Emma A. Gordon [a], Indra D. Sahu [b,a], Muhammad Zeeshan Shah [a], Dominik Konkolewicz [a], Gary A. Lorigan [a,*]

[a] Chemistry and Biochemistry Department, Miami University, Oxford, OH 45056, USA
[b] Natural Science Division, Campbellsville University, Campbellsville, KY 42718, USA

ARTICLE INFO

Keywords:
Lipids
SMA
Saturation
Rigidity
Fluidity
Spin label
CW-EPR

ABSTRACT

Membrane bilayers are complex three-dimensional structures whose molecular events in the deep dimensions of membrane lipids are crucial for understanding membrane function. This study investigates the interaction of coexisting membrane domains in terms of hydrophobicity, alkyl chain order, and fluidity using Styrene Maleic Acid (SMA) copolymers as membrane mimics. We employed continuous wave electron paramagnetic resonance spectroscopy (CW-EPR) to characterize the structural dynamic properties of membrane domains without separation. Lipid-spin probe vesicles were prepared using phospholipids with varying degrees of saturation (DOPC, POPC, DMPC, and DSPC) and doxyl spin-labeled phospholipids at different depths (5, 12, and 16-doxyl PC) as membrane probes. These vesicles were titrated with two SMA polymers of different hydrophobic tail lengths. Dynamic light scattering (DLS) confirmed the formation of Styrene Maleic Acid lipid nanoparticles (SMALPs). CW-EPR spectroscopy was used to characterize the dynamic properties of vesicles incorporated into the SMALP systems. Analysis of the CW-EPR spectral line shape data revealed that the hydrophobic tail of SMA, the degree of lipid saturation, and the length of phospholipids significantly affect membrane fluidity and alkyl chain ordering, as well as lipid interactions. Notably, samples containing DSPC, a fully saturated longer-chain phospholipid, and those containing SMA exhibited increased rigidity of motion, reduced fluidity, and improved ordering of the alkyl chain in the membrane. This study provides crucial insights into the molecular dynamics of membrane bilayers and the impact of SMA copolymers on membrane properties, contributing to our understanding of fundamental membrane functions such as lateral movement of proteins and lipids.

1. Introduction

Membrane proteins represent one-third of proteins in living organisms and pose so much importance in cell-cell signaling and recognition roles, ion transport, immune response, and other biological processes, making them critical drug targets [1,2]. Characterizing membrane proteins has been challenging due to their environment which consists of an innate heterogeneous lipid bilayer and water. This environment introduces solubility, stability, purification, crystallization, and overexpression challenges. To retain the protein's native conformation and perform accurate structural characterization, membrane proteins need to be incorporated in a native membrane mimetic environment [3–6].

Different classes of native-like membrane mimetics such as micelles, bicelles, liposomes, and membrane scaffold protein-based nanodisc have been developed for the structural and functional studies of membrane proteins [7,8]Each membrane-mimetic environment has its advantages and limitations [9]. Detergent micelles are widely used for solubilizing membrane proteins, providing high-resolution structure analysis via solution Nuclear Magnetic Resonance (NMR) spectroscopy due to their smaller size. Still, they can denature or misfold proteins due to an inconsistency with respect to the hydrophobic membrane [9,10]. Bicelles consist of long and short-chain lipids that can assemble into a disk shape allowing both transmembrane proteins and hydrophobic bilayer interiors to be studied [11]. Bicelles are artificial lipid bilayers, and their major limitations are that only a few lipid combinations can form bicelles which makes it very difficult to study a wide range of membrane proteins in them and protein perturbation can be caused by the shape and size of bicelles [9,12]. Using liposomes or vesicles is quite challenging as they are made of different phospholipid lamellae which can cause misfolding of protein due to solubility problems [12,13].

* Corresponding author.
E-mail address: lorigag@miamioh.edu (G.A. Lorigan).

https://doi.org/10.1016/j.bbamem.2025.184424
Received 13 December 2024; Received in revised form 14 April 2025; Accepted 14 May 2025
Available online 22 May 2025

Nanodiscs based on membrane scaffold proteins (MSP) have been shown to enhance lipid stability compared to other bilayer mimetics [14]. However, a drawback of using nanodiscs is that the protein must be solubilized in detergent before being incorporated into the nanodisc, and the absorbance of the membrane scaffold protein can interfere with those of the membrane protein of interest [9] Further, these MSPs used in making the disc can sometimes result in interference in other spectroscopic signals received from the membrane protein of interest [14–16].

Polymers have been used in many studies to form effective biomimetic membrane nanodiscs that are effective [16,17]. Styrene maleic acid copolymer (SMA) interacts with the lipid-bilayer structure and can be formed in solution [18]. Unlike nanodiscs that need MSPs, SMA can solubilize membrane proteins and act as the native environment mimetic of the protein through the formation of a narrow distribution of lipid nanoparticles. These nanodiscs are often called styrene maleic acid copolymer lipid nanoparticles (SMALPs), and the SMALPs can solubilize membrane proteins without the use of detergents [9,19–21]. This disc-like structure gives access to both intra and extracellular membrane lipids and there is a high degree of homogeneity in the size of these SMA-stabilized lipid samples. Several biophysical approaches have been employed to characterize nanodiscs, which include dynamic light scattering (DLS) [20], NMR [21], transmission electron microscopy (TEM) [19–21], and electron paramagnetic resonance (EPR) [18,22].

It is also important to identify the molecular events that occur in the deep dimension of membrane lipids since the membrane domain is not two-dimensional. The interaction of coexisting membrane domains can be studied in terms of hydrophobicity, alkyl chain order, and fluidity. EPR spectroscopy is a relevant biophysical technique that can characterize the mobility within a membrane complex without separation or extraction of the membranes [23]. CW-EPR spectroscopy is a long-standing method to analyze the dynamics in the physical structures of proteins and lipids from an external molecule being introduced onto these molecules. These external molecules are spin probes, and their dynamics and environment are monitored by changes in CW-EPR spectral lineshape [24]. Nitroxide spin-labeled lipids such as the doxyl-pcs are designed to probe the membrane at various depth [25]. Study shows that the doxyl-pc lipids are distributed and approximately localized in the raft and bulk domain [23]. The raft domain, being the rigid domain, contains cholesterol and the 510 doxyl-pcs while the fluidic bulk domain contains the 16-doxyl-pcs. The 12-doxyl-pc is presumably located somewhere between both domains which can be characterized via EPR spectroscopy as well [23].

When a SMA polymer is introduced, the perturbation on the acyl chain can also be detected via EPR spectroscopy by incorporating Phosphatidylcholine based (PC-based) nitroxide spin labels affixed in various carbons in the hydrocarbon chain. Previously, CW-EPR spectroscopy has been used to determine how the introduction of RAFT-synthesized SMA affects the acyl chain perturbation of lipid bilayers through the attachment of PC-based nitroxide spin-labeled lipids of the 5th, 12th, and 16th positions along the acyl chain of the lipid bilayer to examine perturbation on 1-palmitoyl-2-oleoyl-glycero-3-phosphocholine (POPC) lipid [18]. They reported that the EPR spectra of SMALP samples displayed a higher rigidity at position 12 compared to positions 5 and 16 but the effect of this perturbation on lipid saturation is yet unknown [18].

Previous studies suggest that membrane proteins have a strong engagement with their lipid environment hence the composition and structure of the lipid bilayer influence the behavior and functions of the membrane proteins. When forming nanodiscs, the lipid composition also provides an adequate environment for the protein of interest being studied [26]. Therefore, in this work, we focus on lipid and polymer interaction. This study demonstrates the alterations in the physical structure of the lipid bilayer induced by SMA.

We aim to gain more insight into the effect of SMA polymer belts on lipid saturation and membrane fluidity, and rigidity using various depths of spin-labeled lipids. We employ CW-EPR spectroscopy to study the interaction between 3:1 SMA and 2:1 SMA polymers with a molar ratio of 3:1 and 2:1 Styrene to Maleic Acid respectively, and the mixture of spin-labeled nitroxide lipids with other PC-based lipids of different degrees of saturation which are 1,2-dioleoyl-sn-glycero-3-phosphocoline (DOPC), 1-palmitoyl-2-oleoyl-glycero-3-phosphocholine (POPC) and 1,2-dimyristoyl-sn-glycero-3-phosphocholine (DMPC) and 1,2-distearoyl-sn-glycero-3-phosphocholine (DSPC). To compare the effect of lipid saturations on SMALP formation, DOPC was chosen as a fully unsaturated phospholipid with two unsaturated hydrocarbon chains that are 18 carbons long (18:1 Δ9-Cis). POPC (16:0–18:1), a semi-unsaturated lipid, was also chosen to balance the difference between the effect of fully unsaturated lipids to fully saturated lipids. DMPC (14:0) was selected as a commonly studied fully saturated lipid, while DSPC (18:0) was included to provide a comprehensive comparison of chain lengths with DOPC and POPC, as well as to represent full saturation with DMPC, as shown in Fig. 1.

A relative increase in rigidity was found in SMA samples at the 12th position compared to other regions and the mixtures containing fully saturated lipids DMPC and DSPC showed a significant difference in linewidth broadening and lineshape changes compared to solutions containing unsaturated lipids POPC and DOPC through EPR spectroscopy.

2. Materials and method

All phospholipids and spin-labeled lipids were purchased in powder form from Avanti Polar.

2.1. SMA synthesis

SMA samples were synthesized according to a previously published method [21]. Briefly, poly (styrene-*alt*-maleic anhydride-b-styrene) was synthesized by mixing styrene (3.66 g, 35.1 mmol) for 3:1 SMA and Styrene (2.44 g, 23.4 mmol) for 2:1 SMA with maleic anhydride (0.980 g, 10.0 mmol), 2-(Dodecylthiocarbonothioylthio) propanoic acid (0.140 g, 0.4 mmol), Azobis (cyclohexanecarbonitrile) (0.0195 g, 0.008 mmol) and 4.64 g dioxane in a glass vial. This mixture was deoxygenated for 15 min by bubbling with nitrogen and further allowed to polymerize in an oil bath at 90 °C, for 20 h. The polymer was precipitated thrice in excess hexanes at 0 °C to purify it. End-group removal was then conducted by dissolving 4.00 g of polymer in dioxane and further mixed with Benzoyl peroxide (2.40 g, 9.9 mmol), the solution was then deoxygenated and placed in an 80 °C oil bath for 5 h. The polymer was purified in excess cold hexanes three times while dissolving precipitated polymer powder in tetrahydrofuran (THF) each time. Maleic anhydride was then hydrolyzed to maleic acid by dissolving the polymer in minimal THF, a dropwise addition of 4× molar excess of NaOH into the solution, and distilled water (10 mL). The mixture was placed in an oil bath for 24 h at 50 °C. The resulting solution was dialyzed in a 3.5 kDa cutoff tubing in 1 L ultrapure water to remove excess base and THF. The polymer solution was then frozen overnight and lyophilized yielding a soluble white to off-white powder.

2.2. Size exclusion chromatography

3–5 mg of either 2:1 and 3:1 SMA polymer was weighed and dissolved in 1.5 mL of tetrahydrofuran (THF). Two drops of toluene were added to the mixture as a flow rate marker. Subsequently, the solution was filtered through a 0.22 μm filter to remove impurities. Size exclusion chromatography (SEC) was conducted using an Agilent 1260 gel permeation chromatography system. This system included an autosampler, a guard column, and two PLgel MIXED B columns, along with a refractive index detector. THF was the eluent used, running at a constant flow rate of 1 mL/min at 25 °C. Calibration of the SEC system was performed using poly (methyl methacrylate) standards within a

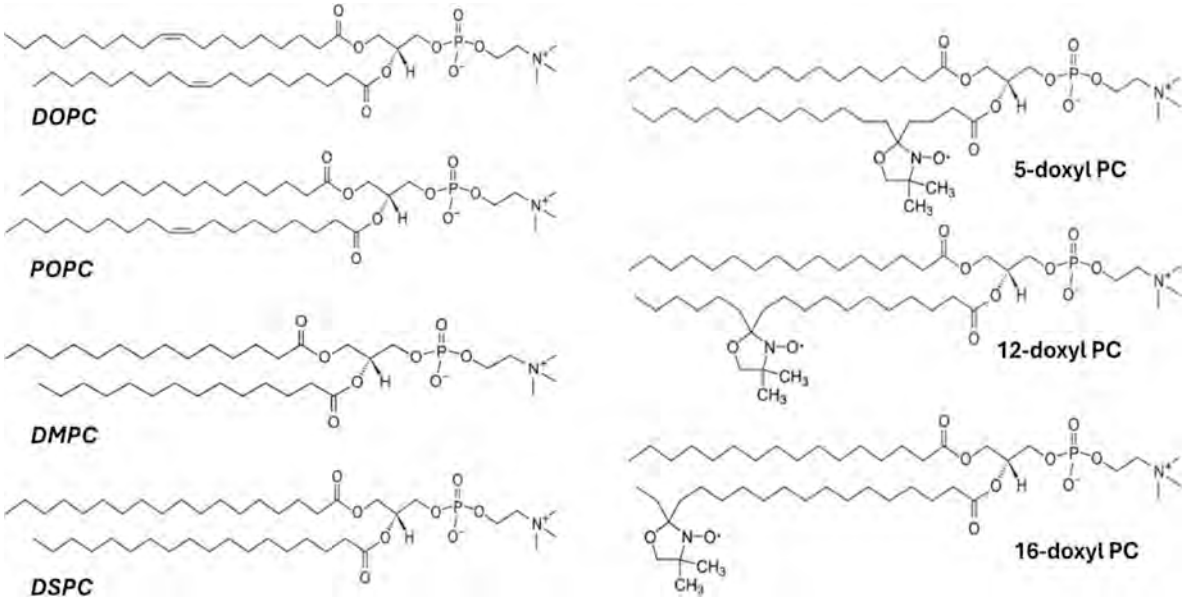

Fig. 1. Chemical structure of the phospholipids and Doxyl spin-label PCs used in the study [25].

molecular weight range of 617,000-1010.

2.3. Vesicle preparation

To characterize spin-labeled lipids and the formation of SMALPS, three different spin-labeled lipids (1 Palmitoyl-2-stearoyl-(5-doxyl)-sn-glycerol-3-phosphocholine), 12-doxyl and 16-doxyl were used alongside four commonly used phospholipids, DOPC, POPC, DMPC and DSPC which possess phosphocholine head groups. These lipids were mixed with spin-labeled lipids to form hybrid vesicles. One set of vesicle samples was composed of a mixture of DOPC with either the 5-doxyl, 12-doxyl, or 16-doxyl spin-labeled lipid. The second set of samples contained a mixture of POPC with either the 5-doxyl, 12-doxyl, or 16-doxyl spin-labeled lipid. Finally, the third and fourth sets of samples contained DMPC and DSPC with either 5-doxyl, 12-doxyl, or 16-doxyl spin-labeled lipid, respectively. In both liposomes and SMA samples, lipid films were generated by incorporating 1 mol% of the spin probe. Previous studies suggest that the ratio of spin probe to lipid is selected to ensure statistically that only one (or fewer) spin-label molecules were present per disc, further ensuring that the EPR spectra will not experience homogenous broadening due to interactions between paramagnetic centers in close proximity [26]. We conducted experiments with lower spin concentrations and determined that incorporating 1 mol% is the optimized spin concentration for one spin per disc to obtain better quality of EPR signals within nanodisc samples, as shown in Fig. S1.

In each sample, powdered phospholipids were mixed with 1 mol% of spin-labeled lipid and dissolved in chloroform. The lipid-spin probe solutions were purged using nitrogen gas to form a thin film and further desiccated overnight to evaporate all chloroform. These samples were hydrated in 2-(4-(2-Hydroxyethyl) piperazine-1-yl) ethane sulfonic acid (HEPES) buffer (20 mM HEPES, 100 mM NaCl, pH 7.0) and brought to a final concentration of 100 mM for the liposome samples. The mixtures were vigorously vortexed and freeze-thawed several times to obtain a homogeneous milky solution to make vesicles. Vesicles were prepared at room temperature for unsaturated lipids and phase transition temperature for the saturated lipids. The size of vesicles was confirmed through dynamic light scattering (DLS), while the free radical interaction of the lipids with the spin label was confirmed using EPR spectroscopy.

2.4. Preparation of SMALPs

The polymers were dissolved in a buffer that contains 20 mM HEPES, 100 mM NaCl, pH 7.0, brought to a final concentration of 3 % mass by volume (m/v), and rigorously vortexed till the solution was clear. The vesicles were titrated with SMA by adding SMA solution dropwise, obtaining the weight ratio ranging from 2:1 to 3:1 (SMA: Vesicle). The newly formed SMALP solutions were properly mixed via slight overnight rotation at 4 °C. SMALP samples were centrifuged at 20,000 rpm for 20 mins to remove excess non-solubilized lipids and polymers while the supernatant was further subjected to DLS and EPR measurements.

2.5. Dynamic light scattering (DLS)

A ZETASIZER NANO Series (Malvern Instruments) was used to perform DLS measurements of samples (40 μL) at 25 °C in a quartz cuvette. Data was collected for 20s and averaged for 12 scans.

2.6. CW-EPR measurements

EPR experiments were conducted at the Ohio Advanced EPR Laboratory. CW-EPR spectra were collected at the X-band on a Bruker EMX CW-EPR spectrometer using an ER041xG microwave bridge and ER4119-HS cavity. Each spin-labeled CW-EPR spectrum was obtained by averaging the signals from 40 field scans, each lasting 42 s with a central field of 3319 G and sweep width of 100 G, modulation frequency of 100 kHz, modulation amplitude of 1 G, and microwave power of 10 mW at room temperature. We analyzed the central linewidth (ΔH) and Spectral linewidth ($2A_{zz}$) of EPR data using the previously outlined method in the literature [18,26,27]. Central linewidth (ΔH) and Spectral linewidth ($2A_{zz}$) were calculated according to the arrows in Fig. 2, where $2A_{zz} = 2A_{max}$ while order parameter was calculated using a formerly established formula:

$$S = 0.5407 \times (A_{max} - A_{min})/a_o \quad (1)$$

$$a_o = (A_{max} + 2A_{min})/3, \quad (2)$$

A_{min} and A_{max} are minimum and maximum hyperfine interaction parameters respectively [27]. Details are shown in Fig. 2. If order parameter (S) equals 1 then the membrane structure is crystal and in

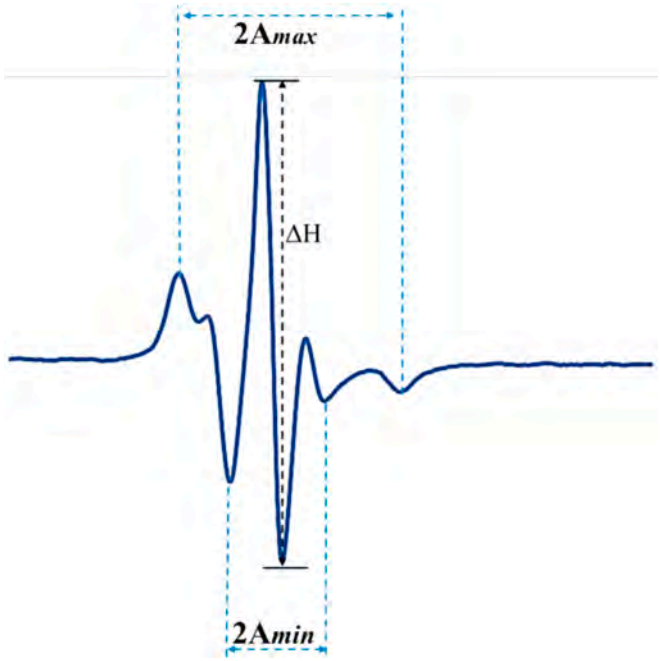

Fig. 2. Central linewidth (ΔH), Spectral linewidth ($2A_{zz}$), A_{max} and A_{min} measurement from EPR spectrum. 2Amax also represents 2Azz.

total disorder when it equals zero.

3. Results

3.1. Size exclusion chromatography (SEC)

The molecular weight distributions of these polymers, derived from size exclusion chromatography, are presented in Fig. 3. The 2:1 styrene to maleic anhydride polymer has a number-average molecular weight (M_n) of 7300 and a dispersity index (M_w/M_n) of 1.3 while the 3:1 styrene to maleic anhydride polymer has M_n of 11,000 and Mw/M_n of 1.3.

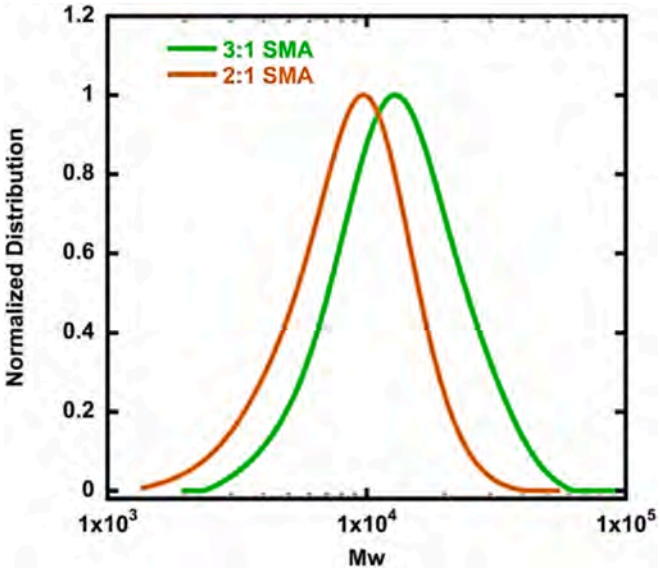

Fig. 3. Molecular weight distribution of 2:1 SMA (Orange) and 3:1 SMA (green). (For interpretation of the references to colour in this figure legend, the reader is referred to the web version of this article.)

3.2. Dynamic light scattering (DLS)

DLS experiment was performed on a ZETASIZER NANO Series (Malvern Instruments) to confirm the effect of the SMA on the size of lipid-spin probe vesicles. Fig. 4 shows the DLS Data of DOPC, POPC, DMPC, DSPC, and their 2:1 and 3:1 SMALP samples.

The DLS data presented in Fig. 4 indicate that the liposome samples, represented in blue, with sizes between 800 nm and 1000 nm, were reduced to less than 30 nm upon the addition of styrene maleic anhydride (SMA). This shows that with a 2:1 ratio of SMA (in orange) and a 3:1 ratio (in green), SMALPs were formed regardless of the lipid saturation level in the samples. This experiment demonstrated that the addition of SMA to lipid-spin vesicles resulted in the formation of lipid nanoparticles of optimal size. No significant difference in particle size was found between spin-labeled and non-spin-labeled SMALP samples based on DLS measurements [18,22,28,29].

It was observed that shorter SMA chains effectively solubilized lipid vesicles, leading to the formation of nanodiscs with high efficiency. In contrast, nanodiscs formed using longer chain SMA exhibited increased stability compared to those formed with shorter chains [30,31]. Specifically, the 2:1 SMA ratio produced smaller nanodiscs of 7–10 nm, while the 3:1 SMA ratio resulted in nanodiscs with diameters of 10–20 nm for unsaturated lipids, as illustrated in Fig. 4A and B. Fig. 4C and D indicated that there was no significant difference in the sizes of SMALPs formed by both polymer chains when applied to fully saturated lipids. This suggests that the particle size of SMALPs is influenced by the ratio of styrene to maleic anhydride (S:MA) for unsaturated lipids, such as DOPC and POPC. However, for saturated lipids like DMPC and DSPC, the ratio did not have a significant effect on particle size during the formation of SMALPs but yielded nanodiscs of approximately the same size regardless of the S:MA ratio used. Also, our results indicate that copolymers do show a preference for solubilizing fluid bilayers and lipids with short or unsaturated acyl chains, as opposed to highly organized membranes containing tightly packed lipids and proteins; this was true for the DLS results for 2:1 SMA, consistent with prior literature findings [32]. Taken together, our findings are consistent with those of Bjornestad and colleagues, who concluded that the size and distribution of SMA in nanodiscs are influenced by temperature, the lipid/copolymer ratio, and lipid type [33]. Notably, the solubilization limit for membranes increases above their melting point, suggesting that defects in gel-phase lipid membranes play a crucial role in membrane fracturing and nanodisc formation [33].

3.3. Continuous wave -electron paramagnetic resonance (CW-EPR) spectroscopy

To understand the interaction of the SMA polymer with different lipid vesicles, we performed CW-EPR experiments on the various lipids (unsaturated lipids: DOPC and POPC; saturated lipids: DMPC and DSPC) containing spin-labeled lipids. CW-EPR lineshape analysis is used to determine the dynamic motion of the spin-labeled PC incorporated into lipid vesicles [18,23,26,34–36]. A broader spectrum represents rigid motion with less fluidity, while sharper lines represent free-spin motion with more fluidity. The 5-doxyl samples have the spin label located close to the lipid head group and are expected to have a broader lineshape due to restricted spin motions by the bulky phosphate group in each phospholipid, as shown in Figs. 5A and 6A. Conversely, 12-doxyl samples are expected to have a less broad lineshape, compared to the 5-doxyl samples, because of the distance between the spin-probe and the lipid head group (Figs. 5B and 6B). Meanwhile, 16-doxyl samples should exhibit a relatively sharp lineshape due to free spin movement and their position at the end of the lipid tail region and in the middle of the bilayer (Figs. 5C and 6C).

The CW-EPR spectra for the unsaturated lipids (DOPC and POPC) from Figs. 5 and 6 are comparable for the liposome samples for each spin labeled carbon position. However, the CW-EPR spectra obtained for

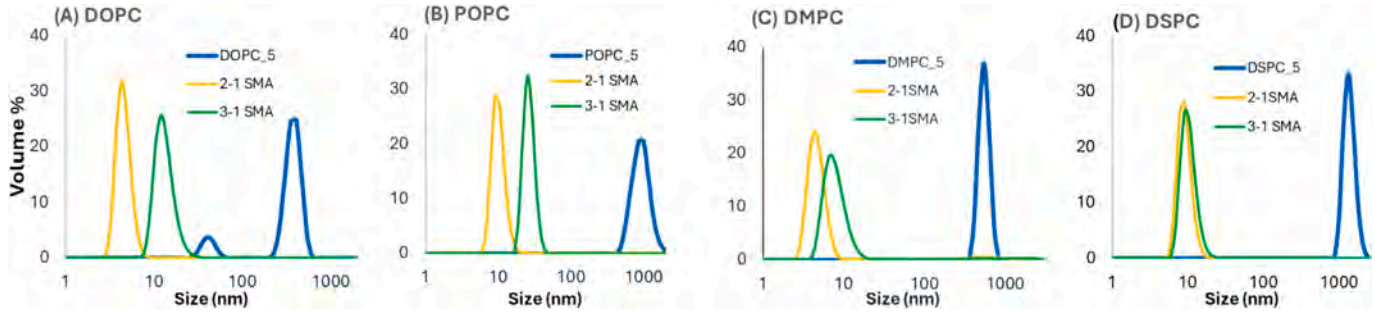

Fig. 4. Representative DLS volume-weighted distributions of the hydrodynamic nanoparticle diameter before and after the addition of 2:1 SMA (orange) and 3:1 SMA (green) for A) DOPC B) POPC C) DMPC, and D) DSPC phospholipids (blue). (For interpretation of the references to colour in this figure legend, the reader is referred to the web version of this article.)

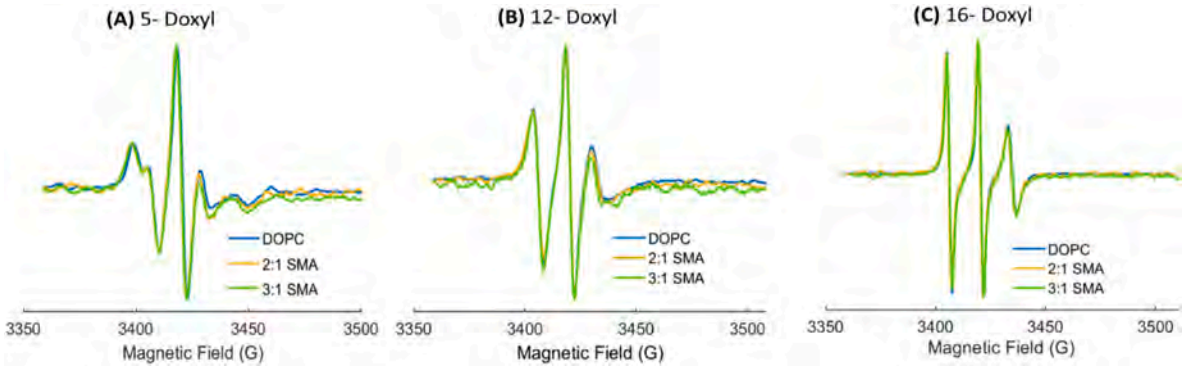

Fig. 5. CW-EPR spectral data for each spin labeled carbon position: (A) 5-, (B) 12-, and (C)16-doxyl PC at 296 K (23 °C) for DOPC lipid vesicles (blue) incorporated in 2:1 SMA (orange) and 3:1 SMA(green). (For interpretation of the references to colour in this figure legend, the reader is referred to the web version of this article.)

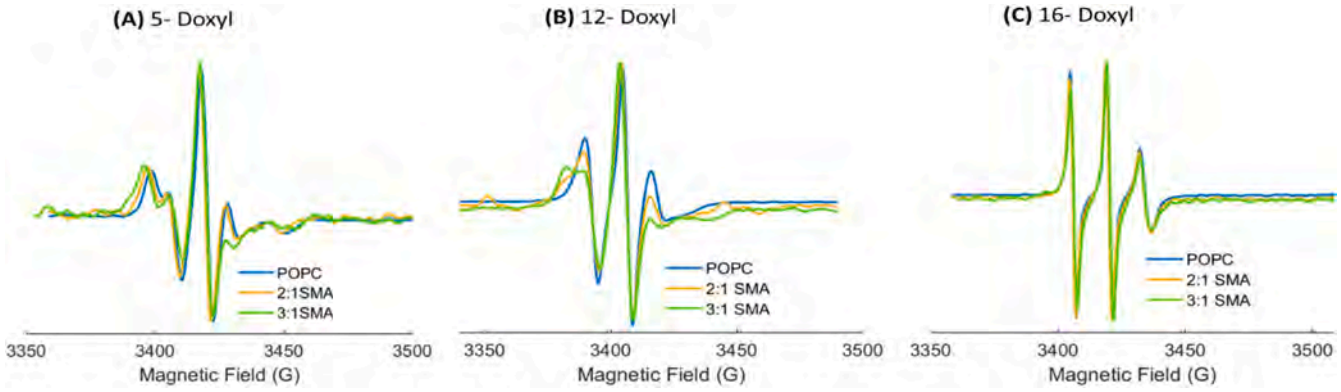

Fig. 6. CW-EPR spectral data for each spin labeled carbon position: (A) 5-, (B) 12-, and (C)16-doxyl PC at 296 K (23 °C) for POPC lipid vesicles (blue) incorporated in 2:1 SMA (orange) and 3:1 SMA(green). (For interpretation of the references to colour in this figure legend, the reader is referred to the web version of this article.)

different SMA samples show a significant difference in lineshape for these liposome samples. Fig. 5 shows the CW-EPR results for DOPC lipids and SMALP samples for the three membrane depths, while Fig. 6 shows the CW-EPR results for POPC lipids and their SMALP samples for the different membrane depths. At the three membrane depths (5-doxyl, 12-doxyl, and 16-doxyl), the EPR lineshape for DOPC vesicle samples was relatively similar for 2:1 and 3:1 SMA samples, as seen in Fig. 5A, B, and C, respectively. The results depicted in Fig. 5 suggest that despite the incorporation of SMA, the lipid membrane environment containing DOPC maintained a native-like (fluidic) state without added rigidity.

Fig. 6 shows the EPR lineshapes for POPC lipids with the 3 spin labeled positions (5-doxyl, 12-doxyl, and 16-doxyl. Fig. 6A shows the lineshape of a POPC vesicle with a 5-doxyl probe, which appeared very similar to the 2:1 SMA sample, with minimal line broadening observed in the 3:1 SMA sample. Similarly, with the 16-doxyl probe (Fig. 6C), the vesicle, 2:1 SMA, and 3:1 SMA samples all exhibited similar lineshape without significant differences. However, at 12-doxyl depth, a significant line broadening was observed in the 3:1 SMA sample, which was even more pronounced than in the 2:1 SMA sample and the vesicle sample (as shown in Fig. 6B). Since these experiments were conducted in the fluid phases of POPC and DOPC, the relatively small increase in broadening of the EPR lineshape can be explained by the fact that POPC is monounsaturated, with one saturated alkyl chain and one unsaturated, compared to DOPC, which has two double bonds with two unsaturated alkyl chains. These double configurations affect the lateral pressure exerted on the lipids by SMA [28,37]. Therefore, POPC-SMA samples appeared more rigid than DOPC-SMA samples because although both are unsaturated lipids, the degree of unsaturation is

higher in DOPC compared to POPC.

CW-EPR spectra of different spin-labeled PCs incorporated into fully saturated lipids DMPC and DSPC lipid vesicles are shown in Figs. 7 and 8. Fig. 7B shows that for the 12-doxyl DMPC samples, the 3:1 SMA sample exhibited the broadest lineshape, followed by the 2:1 SMA sample, which was broader than the liposome sample, but for the 5-doxyl and 16-doxyl samples (Fig. 7A and C), no significant lineshape differences were observed between the SMA samples. These results were further reproduced in Fig. S2. In Fig. 8A, it is evident that there is no significant difference in the lineshapes between the vesicle and SMA samples at 5-doxyl. However, at 12-doxyl and 16-doxyl (Fig. 8B and C), a noticeable line broadening is observed in the SMA samples, contrasting with the vesicle samples. Since DMPC is a fully saturated lipid, it has higher membrane rigidity at positions closer to the head group, i.e., 5 and 12-doxyl, hence the linewidth broadening. However, there could be minimal impact on the spin label far down the chain, i.e., 16-doxyl, because the lipid chain is just 14 carbons long, which prevents strong interactions between the DMPC lipids and the spin label probe at position 16. However, we observed EPR line broadening and rigidity in the membrane with DSPC in all three depths because in addition to being fully saturated, DSPC has a longer acyl chain than that of DMPC, hence the line broadening at 5, 12, and 16-doxyl for the SMA samples. This suggests that the longer acyl chains in DSPC significantly enhance hydrophobic interactions at the 16-doxyl position, surpassing the effects observed with the shorter acyl chains in DMPC. This improved hydrophobicity may have increased the crystallization effect, making DSPC-16 doxyl rigid. The lineshapes of CW-EPR spectra are concurrent with previous literature that DMPC showed a highly increased line-broadening for SMALP samples compared to the liposome samples as shown in Figs. 7 and 8 [18,26,38]. The CW-EPR spectral lineshape broadening observed in the samples may be attributed to a decrease in the motion of the lipid acyl chain when the SMA polymer is present during SMALP formation, resulting in decreased motion of the spin labels. The SMALP system forms due to lateral pressure generated by the interaction of polymer and lipid chains, isolating the individual complex to a smaller size [28]. It is important to note that the level of saturation of the DMPC and DSPC lipids is likely to be a factor here. Additionally, all measurements were taken at room temperature, which is above the gel phase transition temperature of DOPC and POPC, but below that of DMPC and DSPC. However, before taking the measurements, both liposome and nanodisc samples were prepared at temperatures exceeding the phase transition of all lipids.

3.4. Linewidth, spectral width and order parameters

To further probe the dynamic behavior of different lipid vesicles containing 5-,12- and 16-doxyl phospholipids in the presence of SMA polymer, established spectral parameters such as the central linewidth (ΔH_0), and spectral width ($2A_{zz}$) were utilized to analyze our data. Usually, an increase in these parameters indicates reduced mobility of the spin label. Fig. 9 shows a plot of the central linewidth of EPR spectra as a function of the spin-label position at various levels of lipid saturation. The central linewidth ranges from 1.64 G (DOPC_16 doxyl) to 2.83 G (POPC_5 doxyl) for samples of unsaturated lipids without the addition of SMA, and from 1.78 G(DOPC_16_2:1SMA) to 3.55 G with the addition of SMA (POPC_5_3:1SMA). For the fully saturated lipids, vesicle samples without SMA have central linewidth ranging from 1.94 G (DMPC_16 doxyl sample) to 4.18 G (DSPC_5 doxyl sample) and from 2.34 G (DMPC_16_2:1SMA doxyl sample) to 4.62 G (DSPC_5_3:1SMA doxyl sample) with the addition of SMA. Fig. 10 depicts the plot of the spectral width ($2A_{zz}$) of the EPR spectra as a function of the spin label position of the lipids at various levels of saturation. The spectral width ($2A_{zz}$) ranges between 29.3 G (DOPC_16 doxyl) and 50.5 G (POPC_5 doxyl) for samples of unsaturated lipids without the addition of SMA, and between 30.3 G (DOPC_16_2:1SMA) and 55.5 G (POPC_5_3:1SMA) with the addition of SMA. For the fully saturated lipids, the spectral width ($2A_{zz}$) varies between 31.5 G (DMPC_16 doxyl sample) and 61.8 G (DSPC_5 doxyl sample) for vesicle samples without the addition of SMA, and 34.5 G (DMPC_16_2:1SMA doxyl sample) to 63.7 G (DSPC_5_3:1SMA doxyl sample) with the addition of SMA. These data are consistent with previously published literature [18,26]. The increase in these parameters for the fully saturated lipids (DMPC and DSPC) compared to DOPC and POPC indicates decreased motional freedom of the spin label.

In order to further understand the effect of SMA polymer on the organization and flexibility of the lipid bilayer within the membrane vesicles, we determined the order parameters from the CW-EPR spectra obtained for different lipid vesicles containing spin probes in the presence and absence of SMA polymers. Fig. 11 shows a plot depicting the order parameter (S) calculated from the EPR spectra of all four lipids using Eqs. (1) and (2). This plot illustrates how the order parameter varies with the position of the spin label within lipids of different saturation levels. The order parameter, denoted as S, measures the degree of order within the membrane. A value of 1 for S indicates a highly ordered, crystalline structure of the membrane. Conversely, a value of 0 for S suggests that the membrane is in a state of fully dynamic disorder [18,37,39]. This data provides valuable insights into the organization and dynamics of the lipid bilayer within the membrane, shedding light on the impact of lipid saturation levels on the structural arrangement

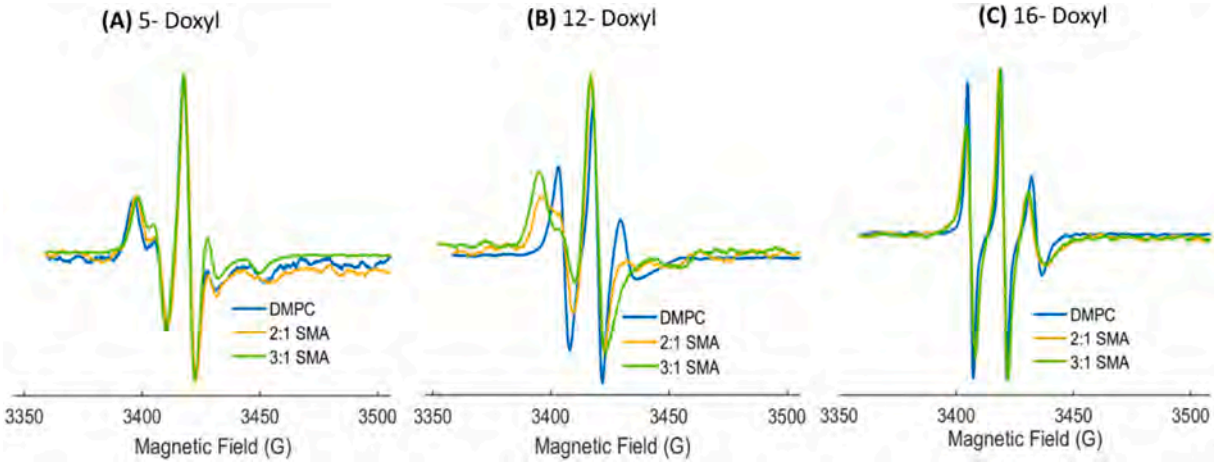

Fig. 7. CW-EPR spectral data for each spin-labeled carbon position: (A) 5-, (B) 12-, and (C)16- doxyl PC at 296 K (23 °C) for DMPC lipid vesicles (blue) incorporated in 2:1 SMA (orange) and 3:1 SMA(green). (For interpretation of the references to colour in this figure legend, the reader is referred to the web version of this article.)

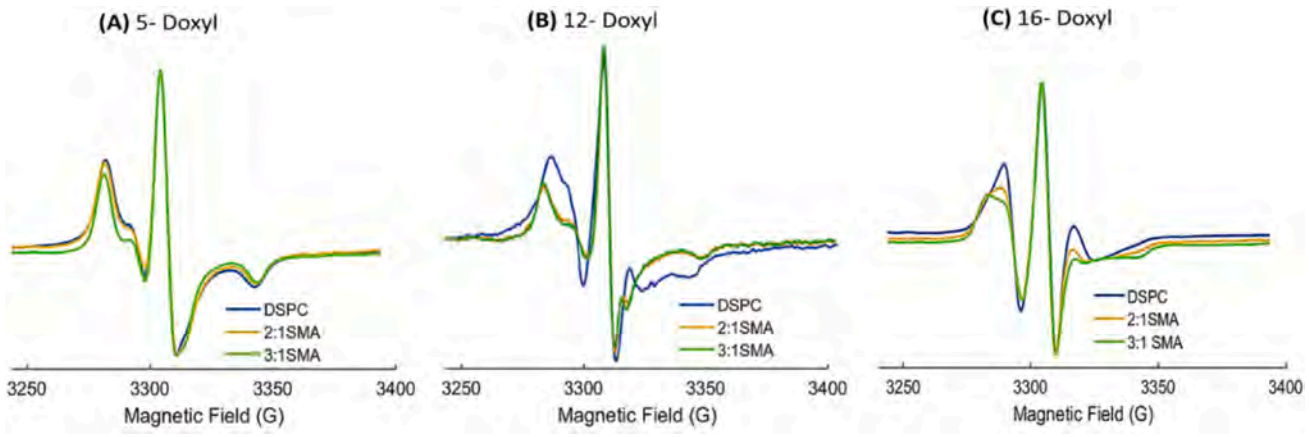

Fig. 8. CW-EPR spectral data for each spin-labeled carbon position: (A) 5-, (B) 12-, and (C)16-doxyl PC at 296 K (23 °C) for DSPC lipid vesicles (blue) incorporated in 2:1 SMA (orange) and 3:1 SMA(green). (For interpretation of the references to colour in this figure legend, the reader is referred to the web version of this article.)

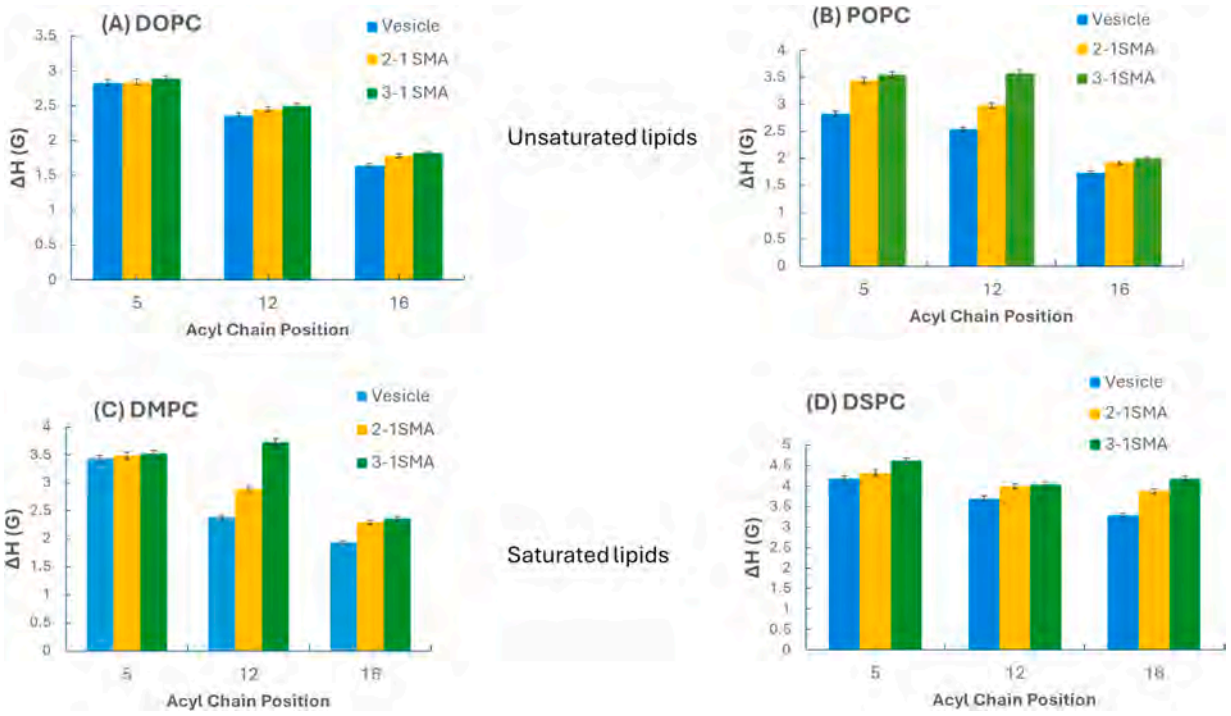

Fig. 9. Central linewidth (ΔH) results of EPR spectra as a function of spin-labeled carbon position in vesicles and with the addition of SMA 2:1 SMA and 3:1 SMA for A) DOPC B) POPC C) DMPC, and D) DSPC phospholipids. The error bars represent uncertainties (standard deviation) that may have arisen from the double batch of sample preparations and data analysis.

and order within the membrane. The order parameter (S) for DOPC vesicle samples was observed to be between 0.07 and 0.58 (in blue), while for 2:1SMA, it was between 0.09 and 0.59 (in orange), and for 3:1SMA, it ranged from 0.10 to 0.60 (in green). This aligns with our EPR lineshape results for DOPC, indicating little to no change in spin motion across all the samples. For POPC samples, the order parameter for vesicles ranged from 0.095 to 0.59, from 0.11 to 0.64 for 2:1 SMA samples, and for 3:1 SMA it ranged from 0.12 to 0.67. For POPC, we observed a 0.1 increase in the order parameter between the vesicle and SMA samples containing the 12-doxyl spin, a trend not observed in the samples with 5-doxyl and 16-doxyl spins. These findings also match our lineshape analysis results, confirming an increased membrane ordering in SMA-POPC samples compared to SMA-DOPC samples.

In addition, for the saturated lipids, the order parameter (S) varied between 0.12 and 0.86 for all the samples without the addition of SMA and ranged from 0.25 to 0.94 when SMA was added. The DMPC showed similar trends to the POPC, with sample ranges of 0.12 to 0.62 for vesicles, 0.23 to 0.71 for 2:1 SMA, and 0.25 to 0.76 for 3:1 SMA. The largest variations for both DMPC and POPC vesicles were observed with 3:1 SMA across spin-probe samples. The 12-doxyl position samples exhibited a greater difference in order level than the other spin positions, which is clearly demonstrated by the gap between the blue and green curves in Fig. 11B and C. However, DSPC displayed a different pattern, with minimal difference between 2:1 and 3:1 SMA samples. It showed a significantly higher order parameter, ranging from 0.62 to 0.94, compared to the vesicle sample's range of 0.27 to 0.86. Additionally, similar high-ordering results were observed at the 12-doxyl and 16-doxyl positions when SMA was added, as reflected in the distance between the blue curve and the other curves (orange and green) in Fig. 11D.

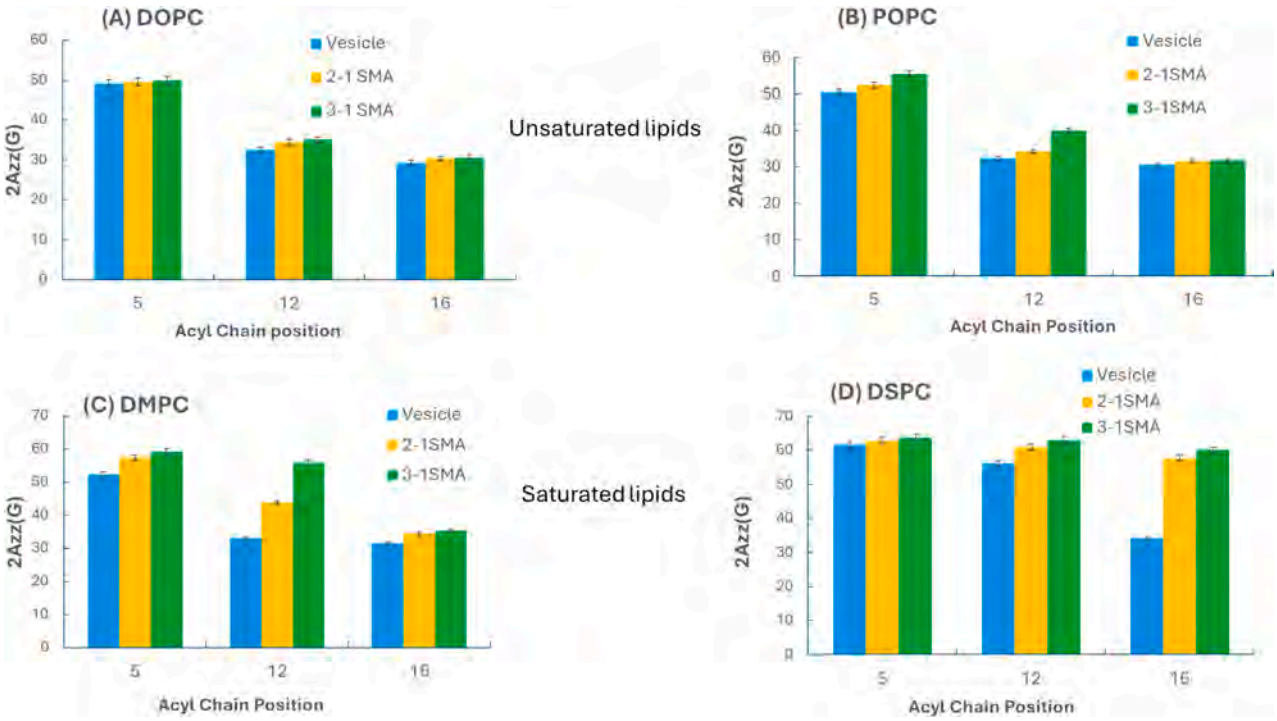

Fig. 10. Spectral linewidth ($2A_{zz}$) results of EPR spectra as a function of spin-labeled carbon position in vesicles and with the addition of SMA 2:1 SMA and 3:1 SMA for A) DOPC B) POPC C) DMPC, and D) DSPC phospholipids. The error bars represent uncertainties (standard deviation) that may have arisen from the double batch of sample preparations and data analysis.

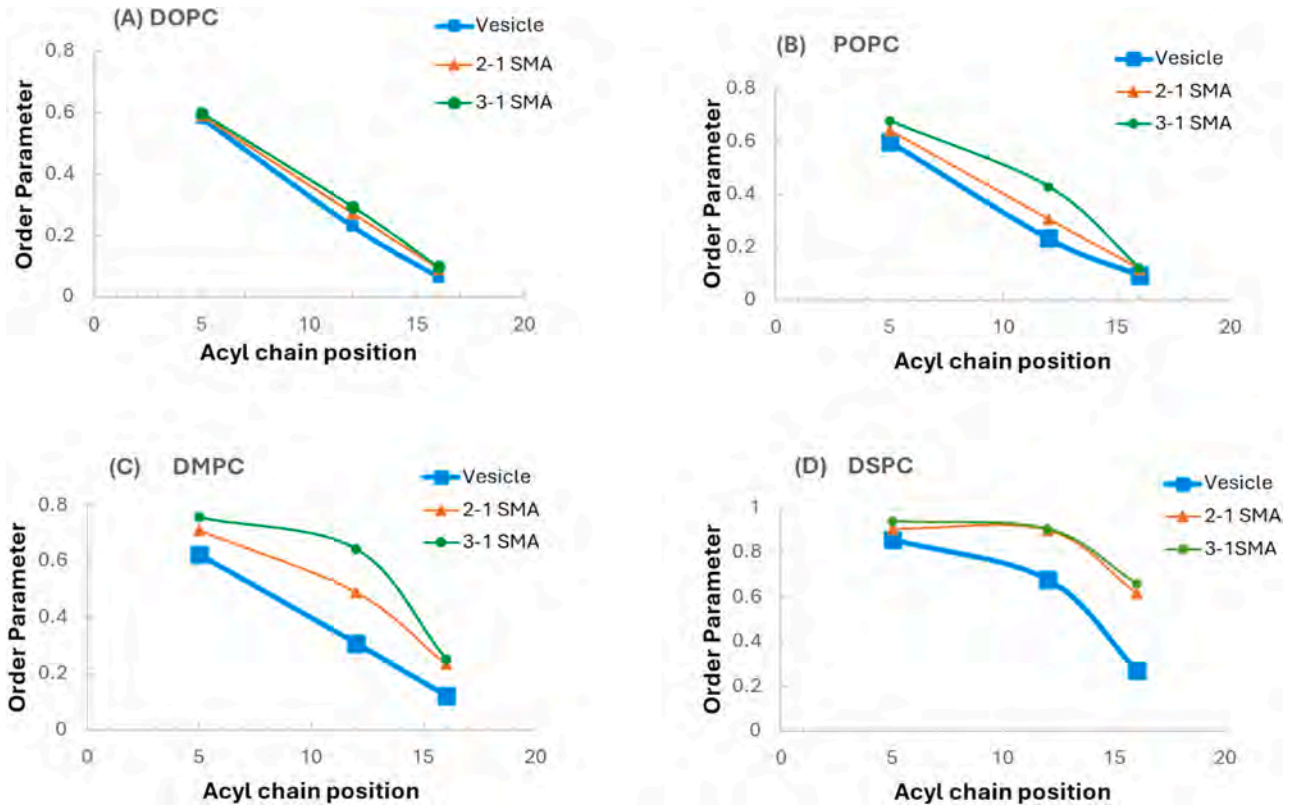

Fig. 11. Order parameter results of doxyl-5,12 and 16 liposomes, 2:1 SMA, and 3:1 SMA samples with A) DOPC B) POPC C) DMPC, and D) DSPC phospholipids.

Our results for POPC and DMPC were consistent with previously published data, while order parameters of DOPC and DSPC with SMA have not been documented in the literature [18,26,34].

4. Discussion

Based on the comparison of EPR spectral parameters at each spin

label position (Figs. 9 and 10), the 12th carbon exhibits the greatest reduction in mobility upon SMA polymer introduction, particularly compared to position 5 in all lipids and position 16 in most lipids except DSPC. This suggests that the fatty acid chain near the polar headgroups of SMALPs remains relatively rigid after SMA incorporation, while carbons in the middle of the fatty acid chain (around the 12th position) experience significantly reduced mobility [18]. Samples in SMA followed a similar trend in hyperfine lineshapes, with 12-doxyl samples showing more complexity and lower mobility, especially in fully saturated lipids. A comparable trend was reported in a study where MSP-incorporated liposomes exhibited reduced motion at the membrane center [26]. Furthermore, no significant dynamic changes were observed at the 16-doxyl position in DOPC, POPC, and DMPC, suggesting an absence of interaction with SMA at this site [18]. However, DSPC showed notable lineshape alterations at position 16, likely due to the length and saturation of its acyl chains. This may be attributed to the lipid's length and its hydrophobic interactions with the doxyl lipid acyl chains. This observation might also imply a minor interaction between the DSPC and the SMA polymer at the 16th position, further suggesting that longer-chain lipids, such as DSPC, impose greater mobility constraints on 16-doxyl compared to shorter-chain lipids like DMPC. In contrast, DMPC, with its shorter alkyl chains, forms fluid and loosely packed bilayers at 16-doxyl, which remain unaffected by SMA incorporation.

As indicated in Fig. 11, the value of the order parameters (S) increased for all acyl chain sites with the addition of SMA, indicating an increase in membrane ordering with the formation of SMALPS. The higher increase in the order parameters of the 12th position in SMALPs than in liposomes suggests that the SMALPs exert pressure on the lipid bilayer during stabilization, causing them to pack into higher ordered structures. Also, it was noticed that the more saturated the lipid, the higher the membrane ordering with or without the addition of SMA, which agrees with previous studies that a membrane with fully saturated lipids is more ordered and less fluidic than a membrane with unsaturated lipids which form kinks and allows for high fluidity and less alkyl ordering [40]This pattern was further observed upon the addition of SMA and 3:1 SMA, which showed more increased ordering, higher rigidity, and lesser fluidity for the fully saturated lipids compared to 2:1 SMA, as seen in Fig. 10C and D, where the DSPC-3:1 SMA sample has an order parameter (S) value of 0.94, very close to 1.

The fluidity of a lipid bilayer is influenced by its composition and temperature. Synthetic bilayers made from a single type of phospholipid transition from a liquid to a solid, crystalline state at a specific phase transition temperature. This temperature is lower, meaning the membrane is harder to crystallize when the hydrocarbon chains are shorter or contain cis-double bonds. Shorter chains reduce interactions between tails, and cis-double bonds create kinks that prevent tight packing, keeping the membrane fluid at lower temperatures [41]. Unsaturated bonds introduce disorder into the chains, reducing the melting point and leading to heightened membrane fluidity and elasticity [42]. These phase characteristics are also largely determined by the degree of the attractive Van der Waals interactions among neighboring lipid molecules. Long-chain lipids increase this interaction, while a high degree of unsaturation increases the membrane fluidity by forming kinks, thereby reducing the Vander Waal force interaction between close-range lipid molecules [41,43]. In addition, because the fatty acid chains of unsaturated lipids are more spread apart, lipid bilayers containing them are thinner than bilayers formed exclusively from saturated lipids [41].

The EPR results correspond to the dynamics of the spin-labeled lipids, and the configuration of EPR spectral lines directly corresponds to the movement characteristics of the spin label. The EPR spectra of 5-doxyl and 12-doxyl reveal broader spectral lines alongside an augmentation in the gap between the outer hyperfine peaks. This phenomenon indicates a restricted movement of the spin labels in contrast to the 16-doxyl sample, while the most significant observed hyperfine splitting is associated with 5-doxyl PC. As expected, the nitroxides situated near the lipid head groups exhibit more constrained reorientation behavior in contrast to the samples where the spin labels are positioned deeper within the lipid bilayer [34]. This is displayed by a broader linewidth seen in 5-doxyl and the higher spectral line widths in 16-doxyl, while 12-doxyl samples are in between.

We investigated the effect of two SMA belts (2:1 and 3:1 SMA) on lipid composition and saturation at various membrane depths while comparing the results with liposome samples that were already well-studied [18,28,44,45]. A more restricted motion of spin-labeled lipids was observed in SMA-encapsulated samples compared to their corresponding liposomes, with 3:1 SMA inducing greater restriction than 2:1 SMA. This effect is likely due to the higher styrene content in 3:1 SMA, which enhances hydrophobicity and promotes stronger interactions with lipid acyl chains, leading to increased lipid ordering. In contrast, the lower styrene content in 2:1 SMA results in a less hydrophobic copolymer, reducing interactions with lipid tails and allowing greater lipid mobility. This also suggests that the frequency of the phenyl chain affects lipid ordering, but further studies are needed in this area. As previously discussed, hyperfine lineshapes exhibited a consistent trend across SMA samples, with 12-doxyl-SMA showing greater complexity and reduced mobility, particularly in fully saturated lipids (DMPC) and in POPC, which is monounsaturated but contains a chain of saturated fatty acid. The different increase in the order parameters between 2:1 and 3:1 SMA nanodiscs observed for DMPC in comparison to POPC may be due to the reduced mobility of fully saturated DMPC lipids when compared to that of monounsaturated POPC lipids.

We have shown that the incorporation of SMA increases the membrane rigidity as the level of lipid saturation increases and has no effect as the level of lipid unsaturation increases. Our result agrees with earlier findings by Scheidelaar et al. that SMA solubilizes short-chain and fully saturated lipids better than long-chain unsaturated lipids at room temperature [46]. Also, our study agrees with Pardo et al. that SMA affects the ordering or disordering of enclosed lipids while increasing membrane rigidity for ordered lipids [47].

Fig. 12 illustrates how membrane rigidity increases with both polymer length and lipid saturation. As the polymer length increases from 2:1 SMA (red) to 3:1 SMA (blue), membrane rigidity increases. Along the horizontal axis, lipid saturation increases, indicating that higher lipid saturation, combined with longer polymer chains, leads to greater membrane stiffness. The red arrow summarizes this relationship, demonstrating that both lipid saturation and polymer chain length are directly proportional to membrane rigidity.

5. Conclusion

Comparing the two polymer belt chains, based on our DLS results, 2:1 SMA formed smaller nanodiscs with unsaturated lipids than 3:1 SMA, while EPR spectral lineshapes showed that 3:1 SMA reduced spin mobility and increased the membrane rigidity of all the lipids more than 2:1 SMA. This suggests that 2:1 SMA is milder in membrane solubilization than 3:1 SMA, which is more hydrophobic as previously published by Grethen et al. [48] Therefore, the length of the polymer belt and its hydrophobicity used for membrane solubilization is a significant factor to be considered when choosing a suitable membrane mimic for biophysical studies of membrane proteins.

This study advances our understanding of lipid composition and the requisite environment necessary for investigating membrane proteins reconstituted in SMA. The results of this study have far-reaching implications for the development of novel pharmaceuticals and biotechnological applications while primarily providing the choices of SMA belt and lipid saturation level needed to achieve a fluidic or rigid membrane environment needed for the specific biophysical study of membrane proteins. Further studies are also required for the temperature-dependent investigation of the behavior of the systems we studied as well as the effect of adding Cholesterol to the system.

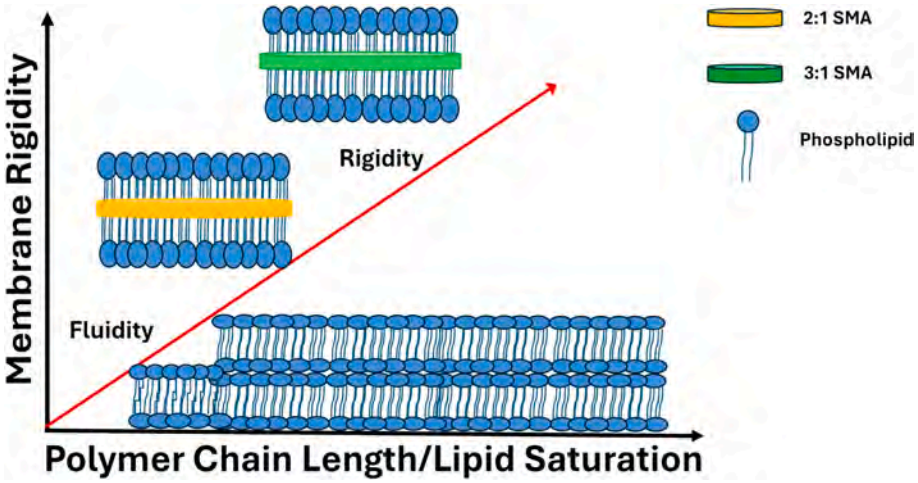

Fig. 12. Schematic representation of how polymer chain length and lipid saturation level affect the fluidity and rigidity of the membrane bilayer. Arrows represent an increase in a parameter. The red arrow shows how rigidity increases as a function of lipid saturation and polymer chain length. (For interpretation of the references to colour in this figure legend, the reader is referred to the web version of this article.)

CRediT authorship contribution statement

Evelyn A. Okorafor: Writing – original draft, Data curation. **Emma A. Gordon:** Data curation. **Indra D. Sahu:** Methodology. **Muhammad Zeeshan Shah:** Methodology, Data curation. **Dominik Konkolewicz:** Supervision, Methodology, Conceptualization. **Gary A. Lorigan:** Writing – review & editing, Supervision, Resources, Project administration, Methodology, Investigation, Funding acquisition, Conceptualization.

Declaration of competing interest

The authors declare that they have no known competing financial interests or personal relationships that could have appeared to influence the work reported in this paper.

Acknowledgments

This work was generously supported by an NIGMS/NIH Maximizing Investigator's Research Award (MIRA) R35 GM126935 06 grant to G.A. L. for SMALP analysis. Indra D. Sahu would also like to acknowledge the support from the National Science Foundation NSF MCB-2040917. DK acknowledges support from NIGMS/NIH under award number R15GM144907 for polymer chemistry.

Appendix A. Supplementary data

Supplementary data to this article can be found online at https://doi.org/10.1016/j.bbamem.2025.184424.

References

[1] Creative Biolabs 2017 Membrane protein overview [Blog post] Https://Www.Creative-Biolabs.Com/Blog/Index.Php/Membrane-Protein-Overview/.
[2] S.C. Bull, A.J. Doig, Properties of protein drug target classes, PloS One 10 (2015) e0117955, https://doi.org/10.1371/journal.pone.0117955.
[3] Y. Arinaminpathy, E. Khurana, D.M. Engelman, M.B. Gerstein, Computational analysis of membrane proteins: the largest class of drug targets, Drug Discov. Today 14 (2009) 1130–1135, https://doi.org/10.1016/j.drudis.2009.08.006.
[4] J.N. Sachs, D.M. Engelman, Introduction to the membrane protein reviews: the interplay of structure, dynamics, and environment in membrane protein function, Annu. Rev. Biochem. 75 (2006) 707–712, https://doi.org/10.1146/annurev.biochem.75.110105.142336.
[5] E.P. Carpenter, K. Beis, A.D. Cameron, S. Iwata, Overcoming the challenges of membrane protein crystallography, Curr. Opin. Struct. Biol. 18 (2008) 581–586, https://doi.org/10.1016/j.sbi.2008.07.001.
[6] V. Yeh, A. Goode, B.B. Bonev, Membrane protein structure determination and characterisation by solution and solid-state NMR, Biology (Basel) 9 (2020) 396, https://doi.org/10.3390/biology9110396.
[7] S. Majeed, A.B. Ahmad, U. Sehar, E.R. Georgieva, Lipid membrane mimetics in functional and structural studies of integral membrane proteins, Membranes (Basel) 11 (2021) 685, https://doi.org/10.3390/membranes11090685.
[8] D. Hardy, E. Desuzinges Mandon, A.J. Rothnie, A. Jawhari, The yin and yang of solubilization and stabilization for wild-type and full-length membrane protein, Methods 147 (2018) 118–125, https://doi.org/10.1016/j.ymeth.2018.02.017.
[9] A.F. Craig, E.E. Clark, I.D. Sahu, R. Zhang, N.D. Frantz, M.S. Al-Abdul-Wahid, C. Dabney-Smith, D. Konkolewicz, G.A. Lorigan, Tuning the size of styrene-maleic acid copolymer-lipid nanoparticles (SMALPs) using RAFT polymerization for biophysical studies, Biochimica et Biophysica Acta (BBA) - Biomembranes 1858 (2016) 2931–2939, https://doi.org/10.1016/j.bbamem.2016.08.004.
[10] C.G. Tate, Practical considerations of membrane protein instability during purification and crystallisation, in: I. Mus-Veteau (Ed.), Methods in molecular biology, heterologous expression of membrane proteins: methods and protocols, 2010, pp. 187–203, https://doi.org/10.1007/978-1-60761-344-2_12.
[11] A. Diller, C. Loudet, F. Aussenac, G. Raffard, S. Fournier, M. Laguerre, A. Grélard, S.J. Opella, F.M. Marassi, E.J. Dufourc, Bicelles: a natural "molecular goniometer" for structural, dynamical and topological studies of molecules in membranes, Biochimie 91 (2009) 744–751, https://doi.org/10.1016/j.biochi.2009.02.003.
[12] T. Raschle, S. Hiller, M. Etzkorn, G. Wagner, Nonmicellar systems for solution NMR spectroscopy of membrane proteins, Curr. Opin. Struct. Biol. 20 (2010) 471–479, https://doi.org/10.1016/j.sbi.2010.05.006.
[13] D.E. Warschawski, A.A. Arnold, M. Beaugrand, A. Gravel, É. Chartrand, I. Marcotte, Choosing membrane mimetics for NMR structural studies of transmembrane proteins, Biochim. Biophys. Acta 1808 (2011) 1957–1974, https://doi.org/10.1016/j.bbamem.2011.03.016.
[14] I.G. Denisov, Y.V. Grinkova, A.A. Lazarides, S.G. Sligar, Directed self-assembly of monodisperse phospholipid bilayer Nanodiscs with controlled size, J. Am. Chem. Soc. 126 (2004) 3477–3487, https://doi.org/10.1021/ja0393574.
[15] T.H. Bayburt, S.G. Sligar, Membrane protein assembly into Nanodiscs, FEBS Lett. 584 (2010) 1721–1727, https://doi.org/10.1016/j.febslet.2009.10.024.
[16] T. Ravula, N.Z. Hardin, A. Ramamoorthy, Polymer nanodiscs: advantages and limitations, Chem. Phys. Lipids 219 (2019) 45–49, https://doi.org/10.1016/j.chemphyslip.2019.01.010.
[17] L.M. Real Hernandez, I. Levental, Lipid packing is disrupted in copolymeric nanodiscs compared with intact membranes, Biophys. J. 122 (2023) 2256–2266, https://doi.org/10.1016/j.bpj.2023.01.013.
[18] A.P. Bali, I.D. Sahu, A.F. Craig, E.E. Clark, K.M. Burridge, M.T. Dolan, C. Dabney-Smith, D. Konkolewicz, G.A. Lorigan, Structural characterization of styrene-maleic acid copolymer-lipid nanoparticles (SMALPs) using EPR spectroscopy, Chem. Phys. Lipids 220 (2019) 6–13, https://doi.org/10.1016/j.chemphyslip.2019.02.003.
[19] E.A. Gordon, Y.B. Richardson, M.Z. Shah, K.M. Burridge, D. Konkolewicz, G. A. Lorigan, Formation of styrene maleic acid lipid nanoparticles (SMALPs) using SMA thin film on a substrate, Anal. Biochem. 647 (2022) 114692, https://doi.org/10.1016/j.ab.2022.114692.
[20] B.D. Harding, G. Dixit, K.M. Burridge, I.D. Sahu, C. Dabney-Smith, R.E. Edelmann, D. Konkolewicz, G.A. Lorigan, Characterizing the structure of styrene-maleic acid copolymer-lipid nanoparticles (SMALPs) using RAFT polymerization for membrane protein spectroscopic studies, Chem. Phys. Lipids 218 (2019) 65–72, https://doi.org/10.1016/j.chemphyslip.2018.12.002.
[21] K.M. Burridge, B.D. Harding, I.D. Sahu, M.M. Kearns, R.B. Stowe, M.T. Dolan, R. E. Edelmann, C. Dabney-Smith, R.C. Page, D. Konkolewicz, G.A. Lorigan, Simple derivatization of RAFT-synthesized styrene–maleic anhydride copolymers for lipid

disk formulations, Biomacromolecules 21 (2020) 1274–1284, https://doi.org/10.1021/acs.biomac.0c00041.
[22] I.D. Sahu, R. Zhang, M.M. Dunagan, A.F. Craig, G.A. Lorigan, Characterization of KCNE1 inside Lipodisq nanoparticles for EPR spectroscopic studies of membrane proteins, J. Phys. Chem. B 121 (2017) 5312–5321, https://doi.org/10.1021/acs.jpcb.7b01705.
[23] Subczynski, W. K., Raguz, M., Widomska, J. Studying lipid organization in biological membranes using liposomes and EPR spin labeling, in: 2010: pp. 247–269. https://doi.org/10.1007/978-1-60761-447-0_18.
[24] E.R. Georgieva, Nanoscale lipid membrane mimetics in spin-labeling and electron paramagnetic resonance spectroscopy studies of protein structure and function, Nanotechnol. Rev. 6 (2017) 75–92, https://doi.org/10.1515/ntrev-2016-0080.
[25] Avanti Polar Lipid Doxyl PC by Avanti Polar Lipid Https://Avantilipids.Com/Product-Category/Stable-Isotopes-Esr-Probes/Doxyl-Pc 2023.
[26] P. Stepien, A. Polit, A. Wisniewska-Becker, Comparative EPR studies on lipid bilayer properties in nanodiscs and liposomes, Biochimica et Biophysica Acta (BBA) - Biomembranes 1848 (2015) 60–66, https://doi.org/10.1016/j.bbamem.2014.10.004.
[27] C. Tan, Y. Zhang, S. Abbas, B. Feng, X. Zhang, W. Xia, S. Xia, Biopolymer–lipid bilayer interaction modulates the physical properties of liposomes: mechanism and structure, J. Agric. Food Chem. 63 (2015) 7277–7285, https://doi.org/10.1021/acs.jafc.5b01422.
[28] M. Orwick-Rydmark, J.E. Lovett, A. Graziadei, L. Lindholm, M.R. Hicks, A. Watts, Detergent-free incorporation of a seven-transmembrane receptor protein into Nanosized bilayer Lipodisq particles for functional and biophysical studies, Nano Lett. 12 (2012) 4687–4692, https://doi.org/10.1021/nl3020395.
[29] M.C. Orwick, P.J. Judge, J. Procek, L. Lindholm, A. Graziadei, A. Engel, G. Gröbner, A. Watts, Detergent-free formation and physicochemical characterization of nanosized lipid–polymer complexes: lipodisq, Angew. Chem. Int. Ed. 51 (2012) 4653–4657, https://doi.org/10.1002/anie.201201355.
[30] J.J. Domínguez Pardo, M.C. Koorengevel, N. Uwugiaren, J. Weijers, A.H. Kopf, H. Jahn, C.A. van Walree, M.J. van Steenbergen, J.A. Killian, Membrane Solubilization by styrene-maleic acid copolymers: delineating the role of polymer length, Biophys. J. 115 (2018) 129–138, https://doi.org/10.1016/j.bpj.2018.05.032.
[31] M. Tanaka, Applications of synthetic polymer discoidal lipid nanoparticles to biomedical research, Chem. Pharm. Bull. 70 (2022) c22-00125, https://doi.org/10.1248/cpb.c22-00125.
[32] M. Overduin, M. Esmaili, Native Nanodiscs and the convergence of Lipidomics, metabolomics, Interactomics and proteomics, Appl. Sci. 9 (2019) 1230, https://doi.org/10.3390/app9061230.
[33] V.A. Bjørnestad, M. Orwick-Rydmark, R. Lund, Understanding the structural pathways for lipid Nanodisc formation: how styrene maleic acid copolymers induce membrane fracture and disc formation, Langmuir 37 (2021) 6178–6188, https://doi.org/10.1021/acs.langmuir.1c00304.
[34] A. Colbasevici, N. Voskoboynikova, P.S. Orekhov, M.E. Bozdaganyan, M. G. Karlova, O.S. Sokolova, J.P. Klare, A.Y. Mulkidjanian, K.V. Shaitan, H.-J. Steinhoff, Lipid dynamics in nanoparticles formed by maleic acid-containing copolymers: EPR spectroscopy and molecular dynamics simulations, Biochimica et Biophysica Acta (BBA) - Biomembranes 1862 (2020) 183207, https://doi.org/10.1016/j.bbamem.2020.183207.
[35] N. Voskoboynikova, P. Orekhov, M. Bozdaganyan, F. Kodde, M. Rademacher, M. Schowe, A. Budke-Gieseking, B. Brickwedde, O.-E. Psathaki, A.Y. Mulkidjanian, K. Cosentino, K.V. Shaitan, H.-J. Steinhoff, Lipid dynamics in Diisobutylene-maleic acid (DIBMA) lipid particles in presence of sensory rhodopsin II, Int. J. Mol. Sci. 22 (2021) 2548, https://doi.org/10.3390/ijms22052548.
[36] R. Bartucci, Spin-Labeling EPR of Lipid Membranes, in: Encyclopedia of biophysics, Springer Berlin Heidelberg, Berlin, Heidelberg, 2013, pp. 2431–2439, https://doi.org/10.1007/978-3-642-16712-6_594.
[37] D. Marsh, Handbook of lipid bilayers, CRC Press, 2013, https://doi.org/10.1201/b11712.
[38] M. Hoffmann, J. Eisermann, F.A. Schöffmann, M. Das, C. Vargas, S. Keller, D. Hinderberger, Influence of different polymer belts on lipid properties in nanodiscs characterized by CW EPR spectroscopy, Biochimica et Biophysica Acta (BBA) - Biomembranes 1863 (2021) 183681, https://doi.org/10.1016/j.bbamem.2021.183681.
[39] J. Seelig, A. Seelig, Lipid conformation in model membranes and biological membranes, Q. Rev. Biophys. 13 (1980) 19–61, https://doi.org/10.1017/S0033583500000305.
[40] K. Hąc-Wydro, P. Wydro, The influence of fatty acids on model cholesterol/phospholipid membranes, Chem. Phys. Lipids 150 (2007) 66–81, https://doi.org/10.1016/j.chemphyslip.2007.06.213.
[41] Alberts, B., Johnson, A., Lewis, J., Raff, M., Roberts, K., Walter, P. The lipid bilayer. Available from: https://www.ncbi.nlm.nih.gov/books/NBK26871/, in: Mol Biol Cell, 4th ed., Garland Science, New York, 2002. https://doi.org/10.1201/9780203833445.
[42] Y. Chi, Alterations in membrane fatty acid unsaturation and chain length in hypertension as observed by 1H NMR spectroscopy, Am. J. Hypertens. 11 (1998) 340–348, https://doi.org/10.1016/S0895-7061(97)00456-1.
[43] W. Rawicz, K.C. Olbrich, T. McIntosh, D. Needham, E. Evans, Effect of chain length and unsaturation on elasticity of lipid bilayers, Biophys. J. 79 (2000) 328–339, https://doi.org/10.1016/S0006-3495(00)76295-3.
[44] S.C.L. Hall, C. Tognoloni, G.J. Price, B. Klumperman, K.J. Edler, T.R. Dafforn, T. Arnold, Influence of poly(styrene- *co* -maleic acid) copolymer structure on the properties and self-assembly of SMALP Nanodiscs, Biomacromolecules 19 (2018) 761–772, https://doi.org/10.1021/acs.biomac.7b01539.
[45] P. Stepien, B. Augustyn, C. Poojari, W. Galan, A. Polit, I. Vattulainen, A. Wisnieska-Becker, T. Rog, Complexity of seemingly simple lipid nanodiscs, Biochim. Biophys. Acta Biomembr. 1862 (2020) 183420, https://doi.org/10.1016/j.bbamem.2020.183420.
[46] S. Scheidelaar, M.C. Koorengevel, J.D. Pardo, J.D. Meeldijk, E. Breukink, J. A. Killian, Molecular model for the Solubilization of membranes into Nanodisks by styrene maleic acid copolymers, Biophys. J. 108 (2015) 279–290, https://doi.org/10.1016/j.bpj.2014.11.3464.
[47] J.J. Domínguez Pardo, C.A. van Walree, M.R. Egmond, M.C. Koorengevel, J. A. Killian, Nanodiscs bounded by styrene-maleic acid allow trans-cis isomerization of enclosed photoswitches of azobenzene labeled lipids, Chem. Phys. Lipids 220 (2019) 1–5, https://doi.org/10.1016/j.chemphyslip.2019.02.002.
[48] A. Grethen, A.O. Oluwole, B. Danielczak, C. Vargas, S. Keller, Thermodynamics of nanodisc formation mediated by styrene/maleic acid (2:1) copolymer, Sci. Rep. 7 (2017) 11517, https://doi.org/10.1038/s41598-017-11616-z.